

Accepted Manuscript

Tautomeric chromoionophores derived from 1-aryloxyanthraquinones and 4'-aminobenzo-15-crown-5 ether: Sandwich complex formation enhanced by interchromophoric interactions

Timofey P. Martyanov, Lubov S. Klimenko, Viacheslav I. Kozlovskiy, Evgeny N. Ushakov

PII: S0040-4020(16)31335-7

DOI: [10.1016/j.tet.2016.12.048](https://doi.org/10.1016/j.tet.2016.12.048)

Reference: TET 28340

To appear in: *Tetrahedron*

Received Date: 10 October 2016

Revised Date: 8 December 2016

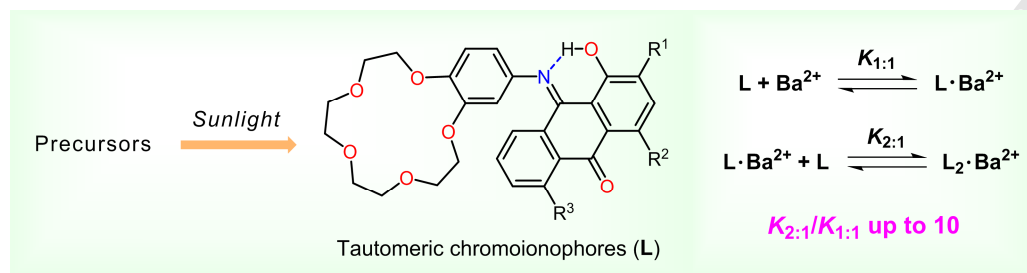
Accepted Date: 19 December 2016

Please cite this article as: Martyanov TP, Klimenko LS, Kozlovskiy VI, Ushakov EN, Tautomeric chromoionophores derived from 1-aryloxyanthraquinones and 4'-aminobenzo-15-crown-5 ether: Sandwich complex formation enhanced by interchromophoric interactions, *Tetrahedron* (2017), doi: 10.1016/j.tet.2016.12.048.

This is a PDF file of an unedited manuscript that has been accepted for publication. As a service to our customers we are providing this early version of the manuscript. The manuscript will undergo copyediting, typesetting, and review of the resulting proof before it is published in its final form. Please note that during the production process errors may be discovered which could affect the content, and all legal disclaimers that apply to the journal pertain.



Graphical Abstract

Tautomeric chromoionophores derived from 1-aryloxyanthraquinones and 4'-aminobenzo-15-crown-5 ether: sandwich complex formation enhanced by interchromophoric interactionsTimofey P. Martyanov^a, Lubov S. Klimenko^b, Viacheslav I. Kozlovskiy^c and Evgeny N. Ushakov^a^a*Institute of Problems of Chemical Physics, Russian Academy of Sciences, Chernogolovka 142432, Russian Federation*^b*Yugra State University, 16 Chehov St., Khanty-Mansiysk 628012, Russian Federation*^c*Talrose Institute for Energy Problems of Chemical Physics (Branch), Russian Academy of Sciences, Chernogolovka 142432, Russian Federation*

Tautomeric chromoionophores derived from 1-aryloxyanthraquinones and 4'-aminobenzo-15-crown-5 ether: sandwich complex formation enhanced by interchromophoric interactions

Timofey P. Martyanov^a, Lubov S. Klimenko^b, Viacheslav I. Kozlovskiy^c and Evgeny N. Ushakov^{a,*}

Address:

^aInstitute of Problems of Chemical Physics, Russian Academy of Sciences, Chernogolovka 142432, Russian Federation

^bYugra State University, 16 Chehov St., Khanty-Mansiysk 628012, Russian Federation

^cTalrose Institute for Energy Problems of Chemical Physics (Branch), Russian Academy of Sciences, Chernogolovka 142432, Russian Federation

Abstract

A series of tautomeric chromoionophores were prepared photochemically from 1-aryloxyanthraquinones and 4'-aminobenzo-15-crown-5 ether. All the synthesized dyes can bind strontium and barium cations as sandwich-type 2:1 ligand–metal complexes that show higher stability constants ($K_{2:1}$) than the corresponding 1:1 complexes ($K_{1:1}$), the $K_{2:1}/K_{1:1}$ ratio reaching a value of 10 (in MeCN). The inverse relation, *i.e.* $K_{2:1} < K_{1:1}$, is observed for the related complexes of unsubstituted benzo-15-crown-5 ether. The sandwich complexes were studied by spectrophotometry, ¹H NMR spectroscopy, mass spectrometry, and density functional theory calculations. A correlation was found between the $K_{2:1}/K_{1:1}$ ratio and the number of short stacking contacts in the sandwich complex.

Keywords

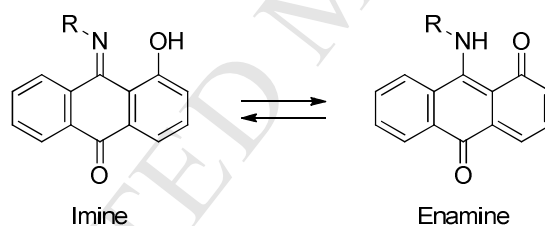
Crown compounds; Anthraquinones; Sandwich complexes; Stacking interactions; Tautomerism

* Corresponding author. E-mail address: e.n.ushakov@gmail.com (E.N. Ushakov).

1. Introduction

The optical properties of tautomeric dyes, dependent on the ratio of tautomeric forms, can be affected by various factors, such as solvent polarity, pH, aggregative state, and photoexcitation.¹ Rational integration of an ionophore into a tautomeric dye can lead to a compound with ion-controllable optical characteristics. Crown ethers are well known as selective ligands for alkali and alkaline-earth metal cations.² They are widely used as building blocks in the design and synthesis of various functionalized compounds, such as photocontrolled molecular receptors³⁻⁵ and optical molecular sensors (chromo- and fluoroionophores).^{4,6,7} Among the variety of chromogenic crown compounds reported in the literature, there are very few examples of tautomeric dyes that can operate as optical sensors for metal ions.⁸⁻¹²

Imine derivatives of 1-hydroxyanthraquinone are known to undergo prototropic tautomerization to exist as an equilibrated mixture of the imine and enamine isomers both in solution and in the solid state (Scheme 1).^{13,14} Recently, we reported the synthesis of a 1-hydroxyanthraquinone-9-imine derivative containing a benzo-18-crown-6 ether moiety.¹⁵ The tautomeric equilibrium of this dye was found to shift toward the imine form in the presence of alkaline-earth metal cations.



Scheme 1. Tautomerism of 1-hydroxyanthraquinone-9-imines.

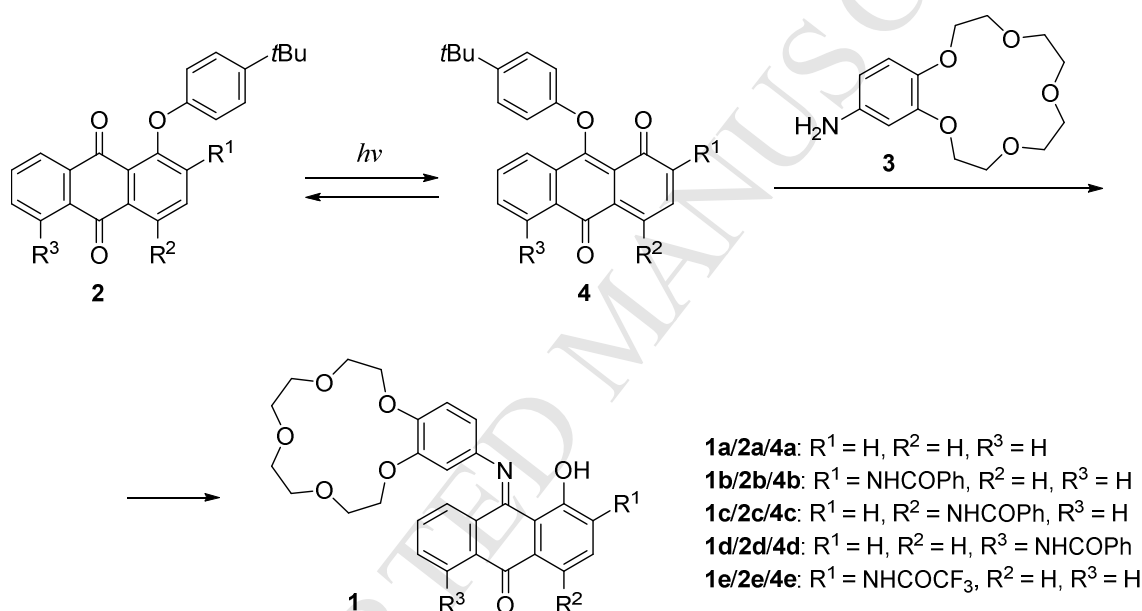
It is well known that 15-crown-5 ethers are able to form sandwich-type 2:1 complexes with relatively large metal ions, such as K^+ , Sr^{2+} , and Ba^{2+} .^{16,17} This feature has been utilized in the design of various ion-selective molecular devices.¹⁸ The sandwich complexes of aromatic crown ethers can have an enhanced stability owing to weak stacking interactions.^{19,20} For crown ether dyes possessing extended π -systems, the effect of stacking interactions on the sandwich complex formation has been little-studied quantitatively.

Here we report on the synthesis of a series of five 1-hydroxyanthraquinone-9-imine dyes containing a benzo-15-crown-5 ether moiety. The complexation of these chromoionophores with alkali and alkaline-earth metal cations was comprehensively studied by spectrophotometry, 1H NMR spectroscopy, mass spectrometry, and quantum chemical calculations. Particular attention was paid to the effect of interchromophoric interactions on the thermodynamic stability of the 2:1 complexes of the dyes with Sr^{2+} and Ba^{2+} .

2. Results and Discussion

2.1 Synthesis

Crown-containing 1-hydroxyanthraquinone-9-imine dyes **1** (Scheme 2) were synthesized photochemically according to the general procedure published previously.²¹ A benzene solution of photochromic 1-aryloxyanthraquinone **2** with aminobenzo-15-crown-5 ether **3** was exposed to sunlight for 6–8 hours. The photoinduced migration of the aryl group in **2** resulted in the *ana*-quinoid isomer **4** possessing a high reactivity toward nucleophilic agents.¹³ The subsequent nucleophilic substitution of the aryloxy group in **4** by the arylamino group of **3** gave the desired products in 58–75% yields. The synthesis of dyes **1a**, **1d**, and **1e** is reported for the first time. Dyes **1b** and **1c**, as obtained by solid-state synthesis, have been described previously.²²



Scheme 2. Synthesis of dyes **1a–e**.

2.2 Spectrophotometric study

The complexation of dyes **1a–e** with alkali and alkaline-earth metal cations in MeCN was studied by spectrophotometric titration (SPT, see the Experimental). Figure 1 shows the SPT data for **1a** and **1c** with Ca(ClO₄)₂ (similar data for dyes **1b**, **1d**, and **1e** are presented in Fig. S1).

Dye **1a** exhibits two broad absorption bands between 350 and 600 nm, assignable to the imine (416 nm) and enamine (464 nm) tautomeric forms (Scheme 1).¹³ The absorption spectral changes observed on the addition of Ca(ClO₄)₂ suggest that the tautomeric equilibrium of **1a** shifts toward the imine isomer. This shift is attributable to the electron-withdrawal effect of the crowned metal ion on the amine nitrogen atom.¹⁵ The same conclusions about the coexistence of two prototropic tautomers and the nature of cation-induced spectral changes hold also for dyes **1b**, **1d**, and **1e**.

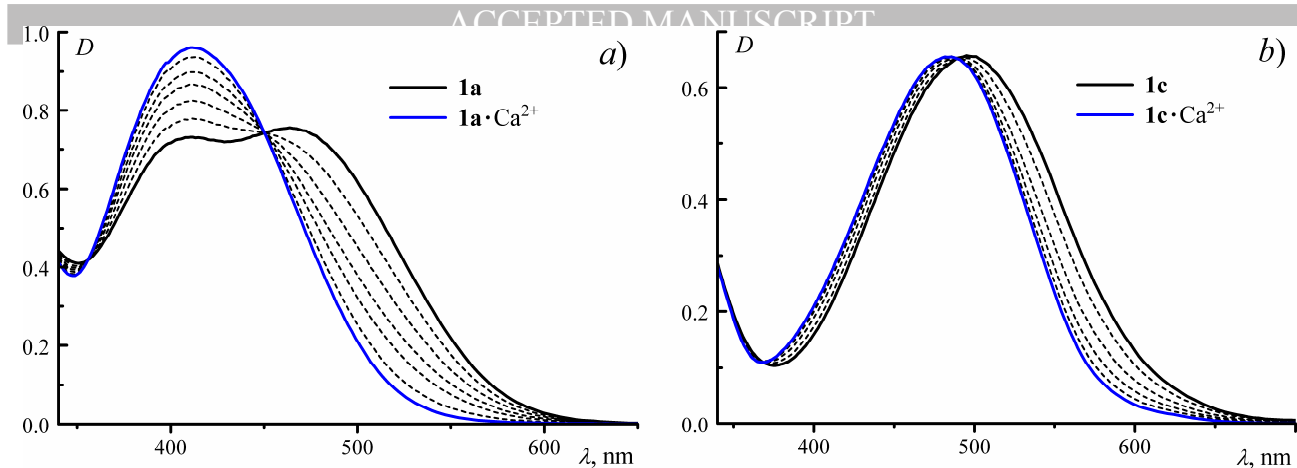


Fig. 1. Spectrophotometric titration data for the systems (a) **1a**–Ca(ClO₄)₂ and (b) **1c**–Ca(ClO₄)₂ in MeCN (4.75 cm cell); the total ligand concentration is (a) 3.0×10^{-5} and (b) 1.25×10^{-5} M, and the total metal concentration varies incrementally (a) from 0 to 4.3×10^{-5} M and (b) from 0 to 3.6×10^{-5} M.

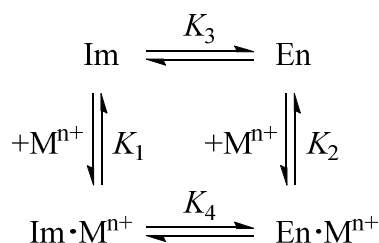
Dye **1c** unlike the others shows a single absorption band peaked at 497 nm, which implies that in MeCN this dye exists almost completely as a single tautomer, presumably, as the imine one. The binding of Ca²⁺ to the crown ether moiety of **1c** induces a hypsochromic shift of the absorption band, indicating a charge-transfer character of the lowest-energy excited state.

The complexation stoichiometry, the complex stability constants, and the absorption spectra of pure complexes for dyes **1** with metal cations were derived from SPT data using the global analysis methods described previously.²³ In most cases, the SPT data were well fitted to one equilibrium:



where L is the dye, Mⁿ⁺ is the metal ion, and $K_{1:1} = [L \cdot M^{n+}] / ([L][M^{n+}])$ is the stability constant of the 1:1 complex.

More rigorously, the 1:1 complexation of the tautomeric dyes should be described by a model involving four light absorbing components, the concentrations of which are determined by the following thermodynamic cycle:



where Im and En are the imine and enamine isomers of the dye, respectively, and K_1 – K_4 are the equilibrium constants. It is obvious that the concentration ratios $[\text{Im}]/[\text{En}]$ and $[\text{Im} \cdot M^{n+}]/[\text{En} \cdot M^{n+}]$ do not depend on the metal cation concentration; therefore, the system can be formally described by the equilibrium of Equation (1) involving the two light absorbing components L and $L \cdot M^{n+}$ with

the concentrations $[L] = (1 + K_3)[Im]$ and $[L \cdot M^{n+}] = (1 + K_4)[Im \cdot M^{n+}]$. The observed stability constant $K_{1:1}$ is related to K_1 , K_3 , and K_4 by the following expression:

$$K_{1:1} = K_1 \{ (K_4 + 1) / (K_3 + 1) \} \quad (2)$$

From the experimental data presented in Figure 1a, we know that $K_3 > K_4$. Then it follows from Equation (2) that $K_{1:1}$ is somewhat lower than the stability constant K_1 of the imine tautomer complex.

For the systems **1**–Sr(ClO₄)₂ and **1**–Ba(ClO₄)₂, the SPT data were well fitted to two equilibria, *viz.* the equilibrium of Equation (1) and the other involving a 2:1 dye–metal complex:



where $K_{2:1} = [L_2 \cdot M^{n+}] / ([L][L \cdot M^{n+}])$ is the stability constant of the 2:1 complex.

Global analysis of the SPT data obtained for the system **1b**–Mg(ClO₄)₂ revealed the formation of a 1:2 dye–metal complex. In this case, the data were fitted to the equilibria of Equations (1) and (4):



where $K_{1:2} = [L \cdot (M^{n+})_2] / ([M^{n+}][L \cdot M^{n+}])$ is the stability constant of the 1:2 complex.

The stability constants of the complexes of dyes **1** with alkali and alkaline-earth metal cations in MeCN, as derived from spectrophotometric titrations, are presented in Table 1. The absorption characteristics of these dyes and their complexes are shown in the same table.

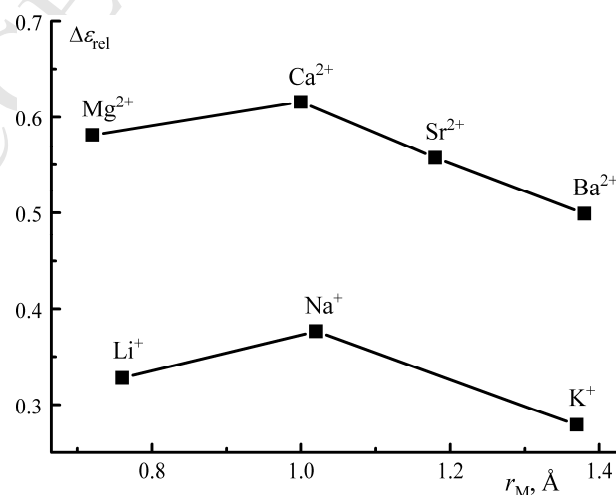
To characterize quantitatively the absorption changes arising from the shift of the tautomeric equilibrium, we used the dimensionless parameter $\Delta \epsilon_{rel} = 1 - \epsilon_{en}(\text{complex}) / \epsilon_{en}(\text{dye})$, where ϵ_{en} is the molar absorptivity (per chromophore) at the absorption maximum λ_{en} of the free enamine tautomer. The λ_{en} values for dyes **1a**, **1b**, **1d**, and **1e** were estimated by fitting the absorption spectrum to a sum of lognormal functions (Fig. S2).

Figure 2 shows the plots of $\Delta \epsilon_{rel}$ vs. the radius of the metal ion (r_M) for the 1:1 complexes of dye **1b** with alkali and alkaline-earth metal cations (similar plots for dye **1a** are presented in Fig. S3). The maxima in these plots correspond to the complexes with Na⁺ and Ca²⁺. This fact suggests that these ions better fit into the cavity of benzo-15-crown-5 ether (B15C5). At the same time, the stability constant $K_{1:1}$ decreases monotonically with an increase in the r_M value both for mono- and divalent cations (Table 1, Fig. 3). The lower values of $\Delta \epsilon_{rel}$ for Li⁺ relative to Na⁺ and for Mg²⁺ relative to Ca²⁺ can be explained by the fact that the Mⁿ⁺–OAr bonds with Li⁺ and Mg²⁺ are weaker because the ionic radii of Li⁺ and Mg²⁺ are smaller than the cavity radius of 15-crown-5 ether.²⁴ However, these ions, due to relatively high charge density, can form stronger bonds with the alkoxy oxygen atoms of B15C5, which results in the larger values of $K_{1:1}$.

Table 1. Stability constants and absorption properties of complexes of dyes **1a–e** with metal cations in MeCN.^a

	$\log K$	λ_{\max}	$\epsilon_{\max} \times 10^{-3}$	$\Delta\lambda$	$\Delta\epsilon_{\text{rel}}$		$\log K$	λ_{\max}	$\epsilon_{\max} \times 10^{-3}$	$\Delta\lambda$	$\Delta\epsilon_{\text{rel}}$
1a		416, 464	5.1, 5.2			1c		497	11		
1a ·Li ⁺	4.56	416	5.77	0	0.144	1c ·Li ⁺	4.46	489	11.24	-8	
1a ·Na ⁺	3.93	416	5.90	0	0.202	1c ·Na ⁺	3.54	491	11.27	-6	
1a ·K ⁺	3.13	418	5.78	+2	0.117	1c ·K ⁺	3.07	493	11.19	-4	
1a ·Mg ²⁺	6.22	412	6.63	-4	0.489	1c ·Mg ²⁺	6.02	485	11.05	-12	
1a ·Ca ²⁺	5.71	410	6.66	-5	0.490	1c ·Ca ²⁺	5.55	482	11.01	-15	
1a ·Sr ²⁺	5.40	412	6.50	-4	0.429	1c ·Sr ²⁺	5.20	485	11.13	-12	
(1a) ₂ ·Sr ²⁺	5.47	417	6.23	+1	0.363	(1c) ₂ ·Sr ²⁺	5.98	491	9.96	-6	
1a ·Ba ²⁺	5.06	413	6.32	-3	0.366	1c ·Ba ²⁺	4.93	485	11.44	-12	
(1a) ₂ ·Ba ²⁺	5.42	417	6.24	+1	0.373	(1c) ₂ ·Ba ²⁺	5.95	493	9.99	-4	
1b		435	8.4			1d		416	9.4		
1b ·Li ⁺	4.33	430	9.21	-5	0.328	1d ·Ca ²⁺	5.75	419	10.96	+3	0.427
1b ·Na ⁺	4.12	429	9.33	-6	0.376	1d ·Sr ²⁺	5.50	419	10.70	+3	0.368
1b ·K ⁺	3.09	430	8.90	-5	0.279	(1d) ₂ ·Sr ²⁺	5.80	423	9.82	+7	0.290
1b ·Mg ²⁺	6.13	424	9.68	-11	0.581	1d ·Ba ²⁺	4.97	419	10.67	+3	0.298
1b ·(Mg ²⁺) ₂	1.04	412	7.66	-23		(1d) ₂ ·Ba ²⁺	5.57	423	9.73	+7	0.325
1b ·Ca ²⁺	5.55	424	9.73	-11	0.616	1e		474	6.5		
1b ·Sr ²⁺	5.01	424	9.64	-11	0.557	1e ·Ca ²⁺	5.42	415	7.93	-59	0.632
(1b) ₂ ·Sr ²⁺	5.96	430	8.40	-5	0.508	1e ·Sr ²⁺	5.10	415	7.69	-59	0.566
1b ·Ba ²⁺	4.82	426	9.54	-9	0.499	(1e) ₂ ·Sr ²⁺	5.55	422	7.13	-52	0.528
(1b) ₂ ·Ba ²⁺	5.70	429	8.46	-6	0.526	1e ·Ba ²⁺	4.84	416	7.50	-58	0.504
						(1e) ₂ ·Ba ²⁺	5.34	420	7.10	-54	0.536

^a K (M⁻¹) = $K_{1,1}$ for L·Mⁿ⁺ complexes, $K = K_{2,1}$ for (L)₂·Mⁿ⁺ complexes, and $K = K_{1,2}$ for L·(Mⁿ⁺)₂ complexes; the K values are determined to within about $\pm 20\%$; λ_{\max} is the position of the absorption maximum, nm; ϵ_{\max} is the molar absorptivity (per chromophore) at λ_{\max} , M⁻¹cm⁻¹; $\Delta\lambda = \lambda_{\max}(\text{complex}) - \lambda_{\max}(\text{dye})$; $\Delta\epsilon_{\text{rel}} = 1 - \epsilon_{\text{en}}(\text{complex})/\epsilon_{\text{en}}(\text{dye})$, where ϵ_{en} is the molar absorptivity (per chromophore) at the absorption maximum λ_{en} of the free enamine tautomer (the λ_{en} values for **1a**, **1b**, **1d**, and **1e** were estimated by spectral deconvolution to be about 484, 545, 499, and 515 nm, respectively).

**Fig. 2.** Plots of $\Delta\epsilon_{\text{rel}}$ vs. r_M for the 1:1 complexes of dye **1b** with alkali and alkaline-earth metal cations in MeCN; the r_M values are taken from ref.²⁵

In order to analyze the complexing properties of dyes **1**, we used B15C5 as the reference ligand. Table 2 presents the stability constants of the complexes of B15C5 with alkali and alkaline-earth metal cations in MeCN, as determined by the method described for dyes **1** (the data for Mg^{2+} and Ca^{2+} are taken from ref.²⁶).

Table 2. Stability constants and absorption properties of complexes of B15C5 with metal cations in MeCN.^a

	$\log K$	λ_{\max}	$\epsilon_{\max} \times 10^{-3}$	$\Delta\lambda$
B15C5		277	2.6	
B15C5·Li ⁺	5.07	273 278	2.47 2.10	-4
B15C5·Na ⁺	4.24	273	2.25	-4
B15C5·K ⁺	3.48	275	2.45	-2
B15C5·Mg ²⁺	7.2 ^b	—	—	—
B15C5·Ca ²⁺	6.6 ^b	—	—	—
B15C5·Sr ²⁺	6.30	269	1.81	-8
(B15C5) ₂ ·Sr ²⁺	5.84	271	1.76	-6
B15C5·Ba ²⁺	5.81	271	1.95	-6
(B15C5) ₂ ·Ba ²⁺	5.58	271	1.81	-6

^a $K (\text{M}^{-1}) = K_{1:1}$ for $\text{L} \cdot \text{M}^{n+}$ complexes, and $K = K_{2:1}$ for $(\text{L})_2 \cdot \text{M}^{n+}$ complexes; the K values are determined to within about $\pm 20\%$; λ_{\max} is the position of the absorption maximum, nm; ϵ_{\max} is the molar absorptivity (per chromophore) at λ_{\max} , $\text{M}^{-1} \text{cm}^{-1}$; $\Delta\lambda = \lambda_{\max}(\text{complex}) - \lambda_{\max}(\text{ligand})$. ^b Ref.²⁶

The dependencies of $K_{1:1}$ on r_M for B15C5 and dyes **1** show a similar trend (Fig. 3, Tables 1 and 2). The $K_{1:1}$ values for the complexes of **1** with divalent cations are lower by about an order of magnitude than those for the corresponding complexes of B15C5. This fact is attributable to the electron-withdrawal effect of the anthraquinone core on the benzocrown ether moiety of the dye. On the contrary, the $K_{2:1}$ values for the complexes of **1b** and **1c** with Sr^{2+} and Ba^{2+} are higher than those for the corresponding complexes of B15C5.

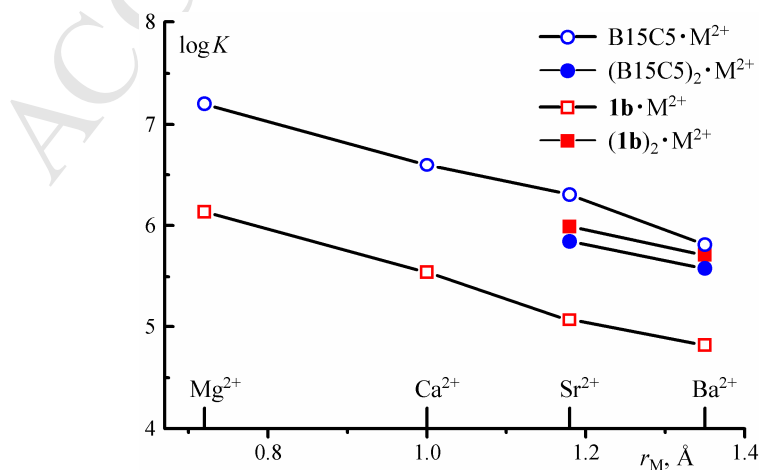


Fig. 3. Plots of $\log K$ vs. r_M for the 1:1 and 2:1 complexes of dye **1b** and B15C5 with alkaline-earth metal cations in MeCN; the r_M values are taken from ref.²⁵

Table 3 presents the ratios of the stability constants and the differences between the Gibbs free energies of formation for the 2:1 and 1:1 complexes of B15C5 and dyes **1** with Sr^{2+} and Ba^{2+} . For B15C5, the relation $K_{2:1} < K_{1:1}$ holds both for Sr^{2+} and Ba^{2+} . The inverse relation is observed for all dyes **1**. The dyes containing a benzoylamino group at the 2 and 4 positions of the 1-hydroxyanthraquinone core (dyes **1b** and **1c**, respectively) demonstrate the largest values of the $K_{2:1}/K_{1:1}$ ratio. In the case of **1c** with Ba^{2+} , this ratio reaches a value of 10. It is most likely that the enhanced stabilities of the sandwich complexes of dyes **1** with Sr^{2+} and Ba^{2+} , as compared with the corresponding 1:1 complexes, result from stacking interactions between the chromophoric moieties.

Table 3. Ratios of the stability constants and differences between the Gibbs free energies of formation for the 2:1 and 1:1 complexes of B15C5 and dyes **1** with Sr^{2+} and Ba^{2+} in MeCN.

Ligand	B15C5	1a	1b	1c	1d	1e	
Substituent		H	2-NHCOPh	4-NHCOPh	5-NHCOPh	2-NHCOCF ₃	
$K_{2:1}/K_{1:1}$	Sr^{2+}	0.35	1.01	8.75	5.97	2.00	2.77
	Ba^{2+}	0.67	2.26	7.60	10.5	3.93	3.17
$\Delta\Delta G$, ^a kJ mol ⁻¹	Sr^{2+}	2.59	-0.029	-5.37	-4.43	-1.72	-2.53
	Ba^{2+}	1.01	-2.02	-5.02	-5.81	-3.39	-2.86

^a $\Delta\Delta G = -RT(\ln K_{2:1} - \ln K_{1:1})$, T = 298 K.

Figure 4 shows the absorption spectra of dye **1b** and complexes $\mathbf{1b}\cdot\text{Sr}^{2+}$ and $(\mathbf{1b})_2\cdot\text{Sr}^{2+}$ (similar data for dyes **1a** and **1c–e** are presented in Fig. S4). The sandwich complex $(\mathbf{1b})_2\cdot\text{Sr}^{2+}$ is characterized by a higher molar absorptivity at $\lambda > 640$ nm in comparison with the free dye and the 1:1 complex (a similar pattern is observed for **1b** with Ba^{2+} , Fig. S5). Presumably, this feature is due to stacking interactions between the benzoyl amino group of one dye molecule and the anthraquinone core of the other in the sandwich complexes involving the enamine tautomer of **1b**. The results of molecular structure calculations (see below) support this supposition.

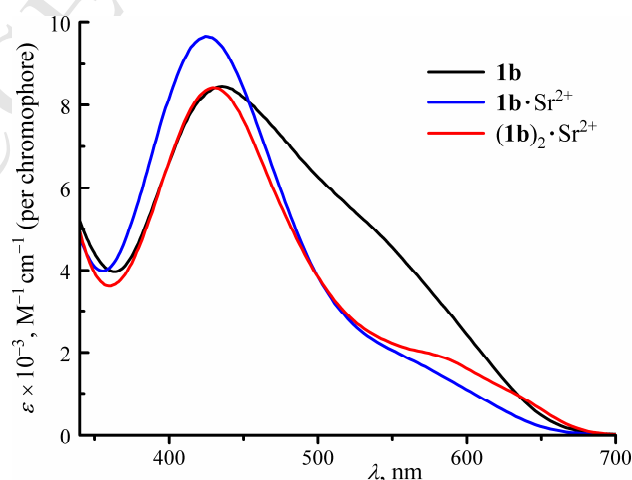


Fig. 4. Absorption spectra of dye **1b** and complexes $\mathbf{1b}\cdot\text{Sr}^{2+}$ and $(\mathbf{1b})_2\cdot\text{Sr}^{2+}$ in MeCN.

An interesting feature of dye **1b** is the ability to form a weak binuclear complex with Mg^{2+} (Table 1). Figure 5 represents the absorption spectra of **1b**, $\mathbf{1b}\cdot\text{Mg}^{2+}$, and $\mathbf{1b}\cdot(\text{Mg}^{2+})_2$ in MeCN. The spectrum of $\mathbf{1b}\cdot\text{Mg}^{2+}$ is similar in shape to the spectra of the 1:1 complexes of **1b** with Ca^{2+} (Fig. S1a), Sr^{2+} (Fig. 4), and Ba^{2+} (Fig. S5b), which indicates that the Mg^{2+} ion in $\mathbf{1b}\cdot\text{Mg}^{2+}$ is bound to the crown ether moiety of the dye. The spectrum of $\mathbf{1b}\cdot(\text{Mg}^{2+})_2$ differs significantly from that of $\mathbf{1b}\cdot\text{Mg}^{2+}$. It is most likely that the binuclear complex forms owing to the binding of Mg^{2+} to the three heteroatoms of the chromophoric moiety of **1b**: the carbonyl oxygen of the benzoylamino group, the hydroxyl oxygen, and the imine nitrogen (see Scheme 3).

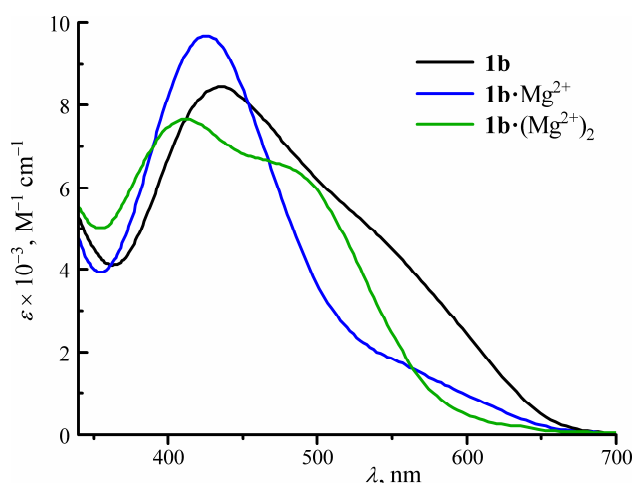
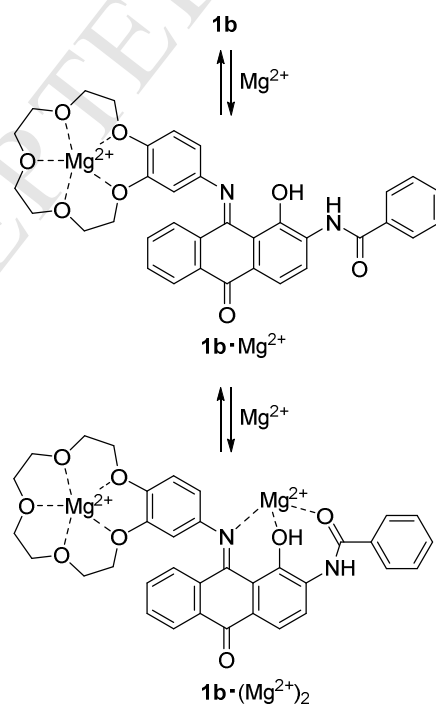


Fig. 5. Absorption spectra of dye **1b** and complexes $\mathbf{1b}\cdot\text{Mg}^{2+}$ and $\mathbf{1b}\cdot(\text{Mg}^{2+})_2$ in MeCN.



Scheme 3. Formation of the binuclear complex $\mathbf{1b}\cdot(\text{Mg}^{2+})_2$.

2.3 NMR spectroscopy

Figure 6 presents the ^1H NMR spectra of the systems $\text{B15C5-Ba}(\text{ClO}_4)_2$ and $\mathbf{1b-Ba}(\text{ClO}_4)_2$ in $\text{MeCN-}d_3$ at different metal-to-ligand molar ratios: $C_M/C_L = 0$ (curves 1), 0.5 (curves 2), and 15 (curves 3), where C_M is the total metal concentration and C_L is the total ligand concentration (in both systems $C_L = 2$ mM). The presence of $\text{Ba}(\text{ClO}_4)_2$ induces significant shifts and broadening of the proton signals of B15C5 and $\mathbf{1b}$. The H-1 signal of B15C5 and the H-2' signal of $\mathbf{1b}$ are shifted upfield at $C_M/C_L = 0.5$ and downfield at $C_M/C_L = 15$. The increase in the C_M/C_L ratio to 100 caused narrowing of all signals in the ^1H NMR spectra of the ligands (Fig. S6). These facts suggest the formation of two different complexes in these systems, *viz.* $\text{L}\cdot\text{Ba}^{2+}$ and $\text{L}_2\cdot\text{Ba}^{2+}$, the latter predominating at $C_M/C_L = 0.5$.

The spectrum of the aromatic protons of free B15C5 is a single multiplet which splits into two multiplets at $C_M/C_L = 0.5$. When the C_M/C_L ratio is increased to 15, the H-1 signal (which is shifted upfield) broadens and moves downfield, so that the positions of the H-1 and H-2 signals are inverted with respect to each other (*cf.* the NMR titration spectra in Fig. S7). It is most likely that the H-1 proton of one ligand molecule in $(\text{B15C5})_2\cdot\text{Ba}^{2+}$ is shielded by the benzene ring of the other, which results in a decrease in the chemical shift (δ) of the H-1 signal.

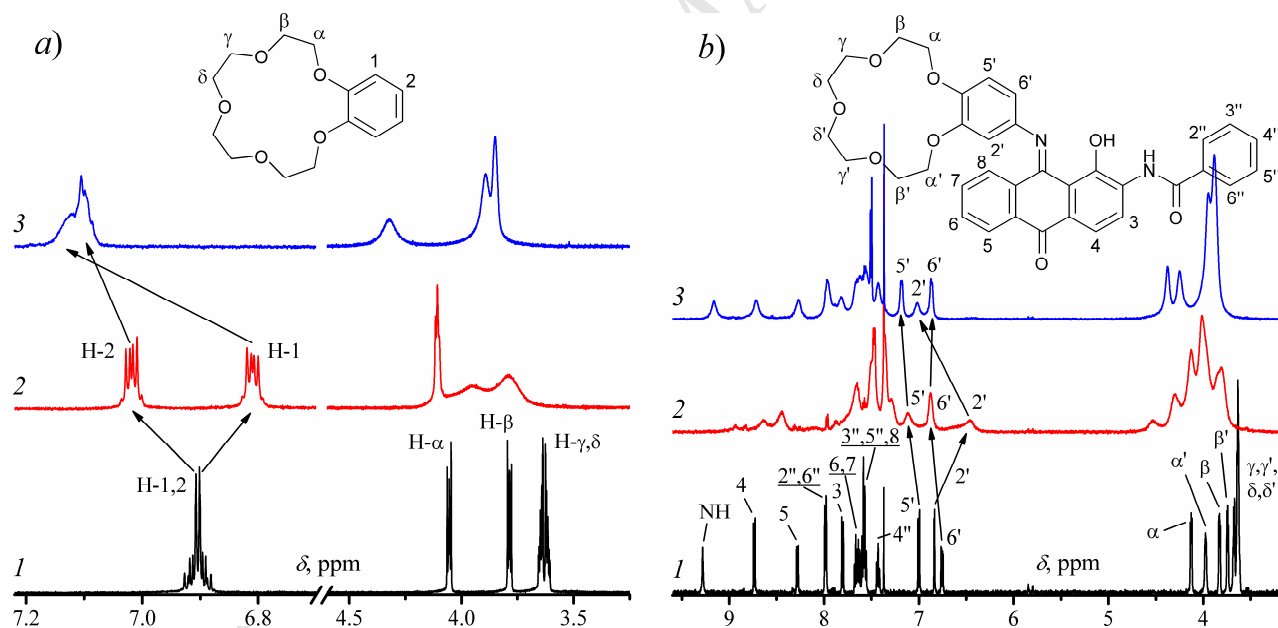


Fig. 6. ^1H NMR spectra of the systems (a) $\text{B15C5-Ba}(\text{ClO}_4)_2$ and (b) $\mathbf{1b-Ba}(\text{ClO}_4)_2$ in $\text{MeCN-}d_3$ at different metal-to-ligand molar ratios: $C_M/C_L = 0$ (curves 1), 0.5 (curves 2), and 15 (curves 3); $C_L = 2$ mM.

The positions of the H-2' and H-6' signals in the ^1H NMR spectra of the $\mathbf{1b-Ba}(\text{ClO}_4)_2$ system are also inverted on changing the C_M/C_L ratio from 0.5 to 15. This indicates that the H-2' proton in $(\mathbf{1b})_2\cdot\text{Ba}^{2+}$ is shielded in the same way as the H-1 proton in $(\text{B15C5})_2\cdot\text{Ba}^{2+}$.

To confirm the reliability of the $K_{2:1}/K_{1:1}$ ratios determined by SPT, we carried out NMR titrations for the systems $\text{B15C5-Ba}(\text{ClO}_4)_2$ and $\mathbf{1b-Ba}(\text{ClO}_4)_2$ in $\text{MeCN-}d_3$. Figure 7 shows the

plots of δ on C_M for some protons in these systems. From these data, it was not possible to determine the stability constants $K_{2:1}$ and $K_{1:1}$ because of their high values, but it was possible to evaluate the $K_{2:1}/K_{1:1}$ ratio. This ratio was estimated by globally fitting the NMR titration curves to the 2:1 complexation model represented by Equations (1) and (3) (details are given in the Experimental). In both cases, the experimental dependencies of δ on C_M are well reproduced by this model, and the best fitted values of $K_{2:1}/K_{1:1}$ are 0.66 for $(\text{B15C5})_2 \cdot \text{Ba}^{2+}$ and 7.73 for $(\mathbf{1b})_2 \cdot \text{Ba}^{2+}$, in perfect agreement with those determined by SPT (Table 3).

The plots of δ on C_M for the systems $\mathbf{1b}$ - $\text{Ba}(\text{ClO}_4)_2$ and B15C5 - $\text{Ba}(\text{ClO}_4)_2$ are similar to each other. In the conversion of the 2:1 complex (low C_M values) into the 1:1 complex (high C_M values), all signals of the aliphatic protons, except the signal of H- β , demonstrate downfield shifts, which is attributable to longer O- Ba^{2+} coordination bonds in the sandwich complex. The distinctive behavior of the H- β signal is presumably due to the fact that the polyether cycle adopts different conformations in the 2:1 and 1:1 complexes.

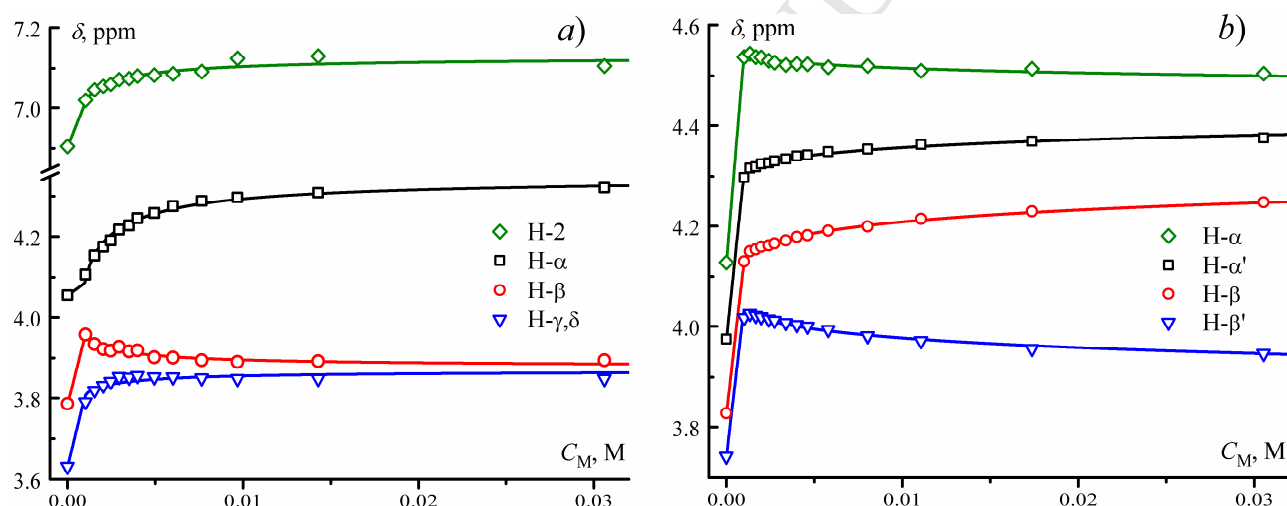


Fig. 7. Plots of δ vs. C_M for some protons in the systems (a) B15C5 - $\text{Ba}(\text{ClO}_4)_2$ and (b) $\mathbf{1b}$ - $\text{Ba}(\text{ClO}_4)_2$ in $\text{MeCN-}d_3$ ($C_L = 2$ mM); the solid curves are from global fits to the 2:1 complexation model represented by Equations (1) and (3).

Figures S8–S10 show the NOESY spectra of the $\mathbf{1b}$ - $\text{Ba}(\text{ClO}_4)_2$ system in $\text{MeCN-}d_3$ - CDCl_3 (4:1, v/v) at $C_L = 2$ mM and $C_M/C_L = 0, 1$, and 100. The NOE interactions observed for dye $\mathbf{1b}$ and complexes $(\mathbf{1b})_2 \cdot \text{Ba}^{2+}$ ($C_M/C_L = 1$) and $\mathbf{1b} \cdot \text{Ba}^{2+}$ ($C_M/C_L = 100$) are depicted schematically in Figure 8. In all three cases, there are the intramolecular cross-peaks of H-8 with H-2' and H-6' (the atom numbering is shown in Fig. 6), indicating rapid interconversion between the two dye conformations associated with the rotation of the benzocrown ether moiety around the Ar-N single bond (*s-cis* and *s-trans*, Fig. 8).

The NOESY spectrum of $\mathbf{1b}$ shows weak cross-peaks of H(hydroxyl) with H-2' and H-6'. In the spectrum of $\mathbf{1b} \cdot \text{Ba}^{2+}$, these cross-peaks are absent, which can be explained by the shift of the

dye tautomeric equilibrium toward the imine isomer (the distances from the hydroxyl hydrogen to H-2' and H-6' are supposed to be larger in the imine isomer than in the enamine one). In the spectrum of $(\mathbf{1b})_2 \cdot \text{Ba}^{2+}$, the cross-peak between H(hydroxyl) and H-2' is also absent, but the main reason for this appears to be a considerable broadening of the H-2' signal (the broadening is due to a great difference in the H-2' chemical shifts between complexes $(\mathbf{1b})_2 \cdot \text{Ba}^{2+}$ and $\mathbf{1b} \cdot \text{Ba}^{2+}$). Compared with the free dye, complex $(\mathbf{1b})_2 \cdot \text{Ba}^{2+}$ is characterized by a more intense cross-peak between H(hydroxyl) and H-6' (its intensity is doubled with respect to the cross-peak between H- α and H-5'). Most likely, it arises from the intermolecular NOE. The results of molecular structure calculations presented below support this hypothesis.

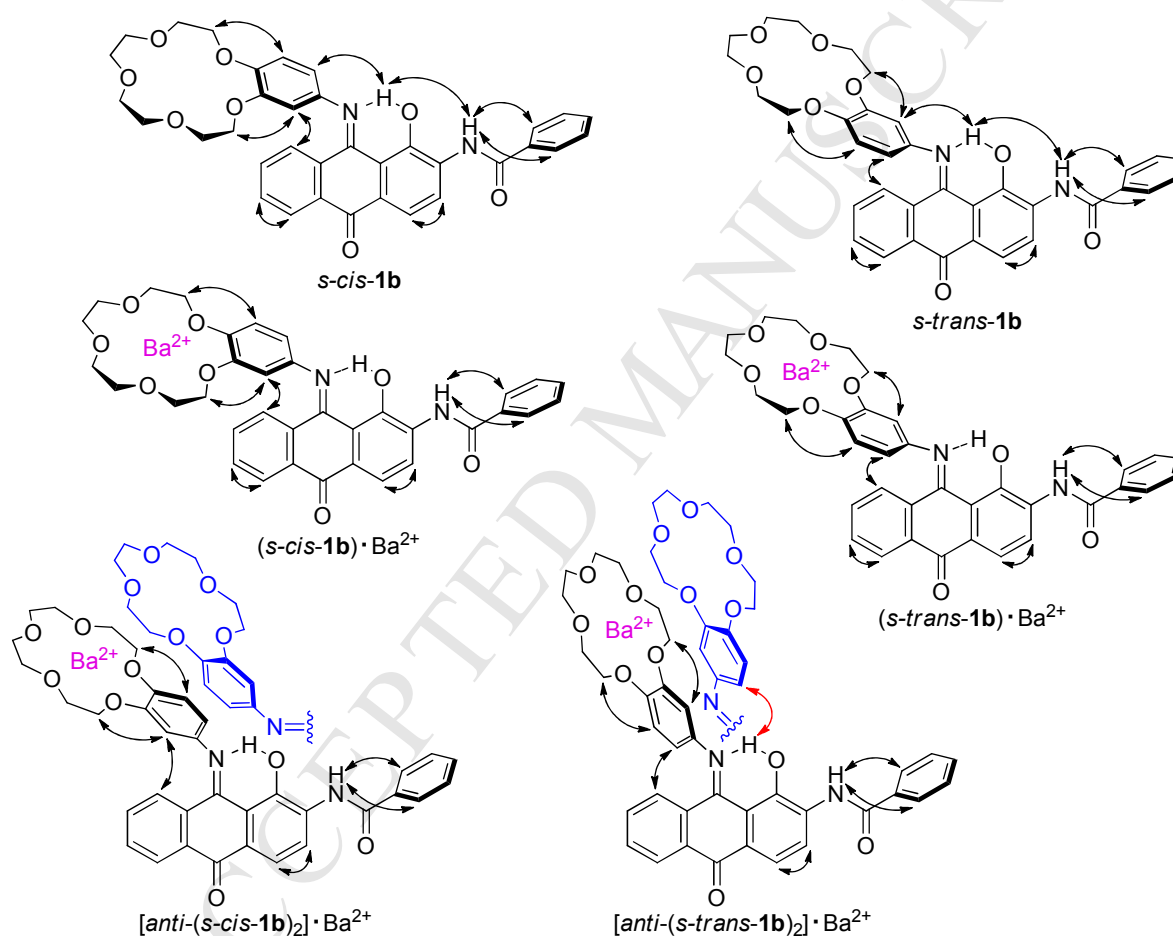


Fig. 8. NOE interactions in different conformers of $\mathbf{1b}$, $\mathbf{1b} \cdot \text{Ba}^{2+}$, and $(\mathbf{1b})_2 \cdot \text{Ba}^{2+}$.

2.4 Mass spectrometry

The complexation of $(\text{BaClO}_4)_2$ with B15C5 and dyes $\mathbf{1b}$ and $\mathbf{1c}$ was investigated by electrostatic spray ionization mass spectrometry (ESSI-MS, see the Experimental). Figures 9 shows the ESSI-MS spectra of the systems B15C5- $(\text{BaClO}_4)_2$ and $\mathbf{1b}$ - $(\text{BaClO}_4)_2$ in MeCN, obtained at a spray voltage of 2.7 kV.

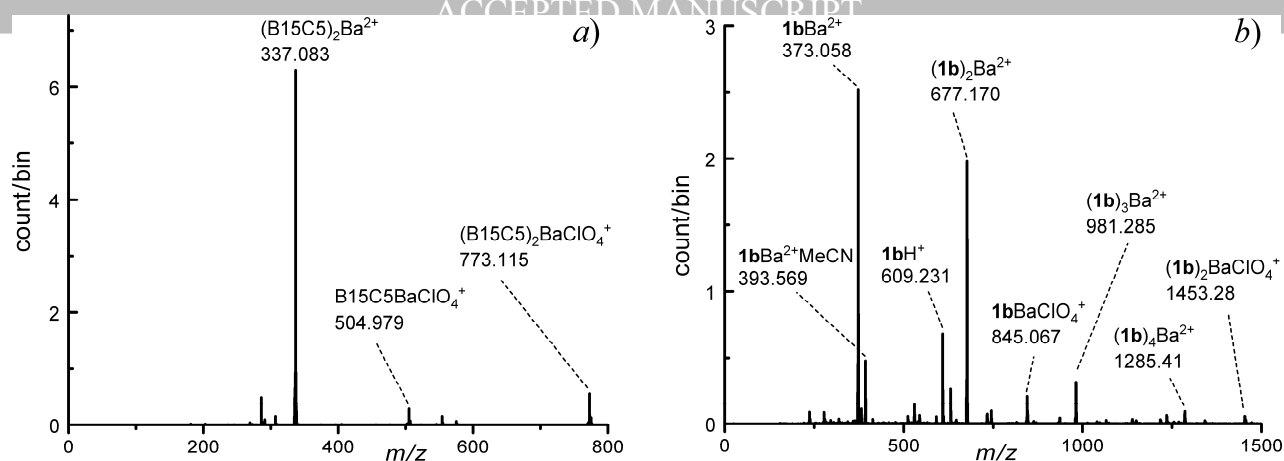


Fig. 9. ESSI mass spectra of the systems (a) B15C5–(BaClO₄)₂ and (b) **1b**–(BaClO₄)₂ in MeCN ($C_L = C_M = 1 \times 10^{-4}$ M), obtained at a spray voltage of 2.7 kV.

In the case of B15C5, the spectrum contains signals from $(\text{B15C5})_2 \cdot \text{Ba}^{2+}$, $(\text{B15C5})_2 \cdot \text{BaClO}_4^+$, $\text{B15C5} \cdot \text{BaClO}_4^+$, and complexes with impurity ions (not denoted). The absence of the signal from the non-associated $\text{B15C5} \cdot \text{Ba}^{2+}$ complex, probably, results from a lower surface activity of this species in comparison with the ion pairs and the non-associated $(\text{B15C5})_2 \cdot \text{Ba}^{2+}$ complex. Due to the lower surface activity, the $\text{B15C5} \cdot \text{Ba}^{2+}$ complex is located in the droplet bulk, not on the surface, which suppresses its release into the gas phase through the droplet fission cascade.²⁷ The decrease in the spray voltage to 150 V led to a significant reduction in the signal intensity of $(\text{B15C5})_2 \cdot \text{Ba}^{2+}$ relative to both $\text{B15C5} \cdot \text{BaClO}_4^+$ and $(\text{B15C5})_2 \cdot \text{BaClO}_4^+$ (Fig. S13) owing to the formation of less charged droplets.

The ESSI-MS spectrum of the **1b**–(BaClO₄)₂ system exhibits the signals from both $(\text{1b})_2 \cdot \text{Ba}^{2+}$ and $\text{1b} \cdot \text{Ba}^{2+}$, which suggests that the difference in the surface activity between these complexes is much less than that between $(\text{B15C5})_2 \cdot \text{Ba}^{2+}$ and $\text{B15C5} \cdot \text{Ba}^{2+}$. The reason for the smaller difference is that dye **1b** contains a bulky hydrophobic moiety. The spectrum shows the signal from a protonated form of dye **1b** (1bH^+). Presumably, this signal appears mainly due to the protonation of $(\text{1b})_2 \cdot \text{Ba}^{2+}$ followed by the dissociation into 1bH^+ and $\text{1b} \cdot \text{Ba}^{2+}$. This presumption is supported by the fact that the decrease in the spray voltage to 150 V caused a significant enhancement of the signal intensity of $(\text{1b})_2 \cdot \text{Ba}^{2+}$ relative to both 1bH^+ and $\text{1b} \cdot \text{Ba}^{2+}$ (Fig. S14). The ESSI-MS spectrum of the system **1c**–(BaClO₄)₂ essentially shows similar features (Fig. S15).

It has been reported that electrospray ionization mass spectrometry can be used to determine stability constants of crown ether–metal cation complexes.^{28–30} In the case of dyes **1b** and **1c**, this method is not suitable for this purpose due to the observed protonation processes.

2.5 Quantum-chemical calculations

The molecular structures of complexes $(\text{1})_2 \cdot \text{Sr}^{2+}$ and $(\text{B15C5})_2 \cdot \text{Sr}^{2+}$ in MeCN were studied using density functional theory (DFT, see the Experimental). The most stable conformations of the

complexes, as calculated by DFT, are shown in Figure 10. The dye molecules in $(\mathbf{1})_2 \cdot \text{Sr}^{2+}$ are present as the *s-trans*-conformers with respect to rotation of the benzocrown ether moiety around the Ar–N single bond. The two 1-hydroxyanthraquinone-imine moieties adopt an *anti*-conformation relative to each other, which was found to be much more stable than *syn*-conformations.

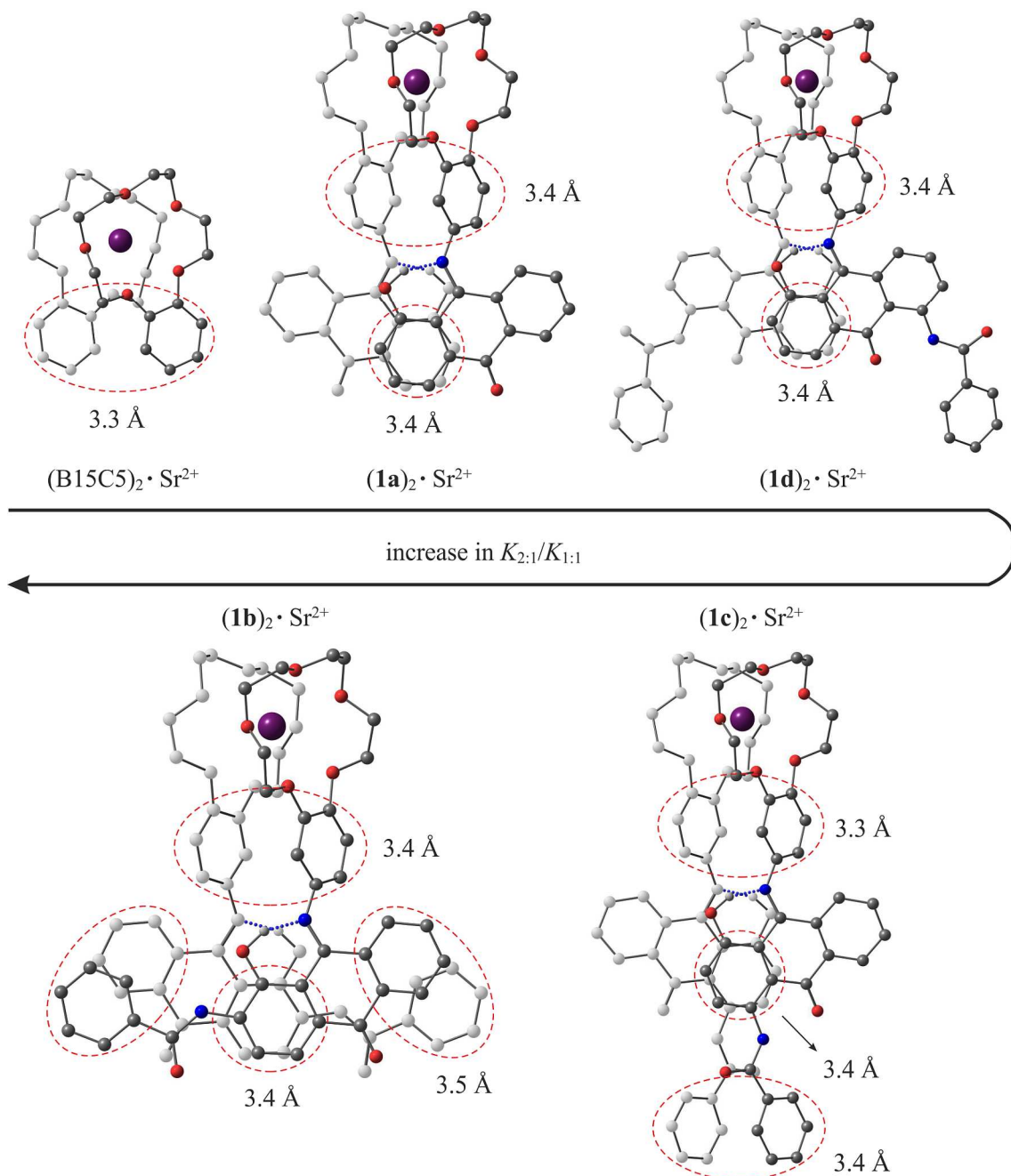


Fig. 10. Most stable conformations of complexes $(\text{B15C5})_2 \cdot \text{Sr}^{2+}$ and $(\mathbf{1a-d})_2 \cdot \text{Sr}^{2+}$ in MeCN, as calculated by DFT; hydrogen atoms are not shown, except the hydroxyl hydrogen.

The calculated sandwich structures are characterized by a different number of short stacking contacts (SC). The SC number varies in the following order: B15C5 (1 SC) < $\mathbf{1a} = \mathbf{1d}$ (2 SC) < $\mathbf{1c}$ (3 SC) < $\mathbf{1b}$ (4 SC). According to experimental data (see the $K_{2:1}/K_{1:1}$ ratios or the $\delta\Delta G$ values in Table 3), the relative stability of the 2:1 complexes of B15C5 and dyes $\mathbf{1a-d}$ with Sr^{2+} with respect

to the corresponding 1:1 complexes increases as follows: $B15C5 < \mathbf{1a} < \mathbf{1d} < \mathbf{1c} < \mathbf{1b}$. That is, there is a correlation between the number of stacking contacts in the sandwich complex and its relative stability.

In the calculated structures $[anti-(s-trans-\mathbf{1})_2] \cdot Sr^{2+}$, the H-2' of one benzocrown unit is in the shielding region of the benzene ring of the other, which agrees with the observed upfield shift of the H-2' signal in the NMR spectrum of the related complex $(\mathbf{1b})_2 \cdot Ba^{2+}$ (Fig. 6).

The intramolecular distances between H-6' and H-8 and between H(hydroxyl) and H-2' in structure $[anti-(s-trans-\mathbf{1b})_2] \cdot Sr^{2+}$ are 2.79 and 2.72 Å, respectively. The fact that the NOESY spectrum of the related complex $(\mathbf{1b})_2 \cdot Ba^{2+}$ does not show the expected cross-peak between H(hydroxyl) and H-2' is due to significant broadening of the H-2' signal.

The intramolecular distance between H(hydroxyl) and H-6' in $[anti-(s-trans-\mathbf{1b})_2] \cdot Sr^{2+}$ is equal to 4.00 Å, whereas the intermolecular distance is just 3.02 Å. Figure S17 represents the *anti-(s-cis)*₂ and *anti-(s-cis,s-trans)* conformations of $(\mathbf{1b})_2 \cdot Sr^{2+}$ calculated by the same method. The relative DFT energies of these conformers with respect to $[anti-(s-trans-\mathbf{1b})_2] \cdot Sr^{2+}$ are about +0.3 and +1.8 kcal/mol, respectively. The intra- and intermolecular distances between H(hydroxyl) and H-6' in the *anti-(s-cis)*₂ conformer (3.56 and 5.78 Å, respectively) are significantly larger than the intermolecular distance between these atoms in the *anti-(s-trans)*₂ conformer. In the non-symmetrical conformer *anti-(s-cis,s-trans)*, the intramolecular distances between H(hydroxyl) and H-6' (3.32 and 3.62 Å) are also larger than 3.02 Å, whereas the shortest intermolecular distance is just 2.35 Å. These facts support the conclusion that the cross-peak between H(hydroxyl) and H-6' in the NOESY spectrum of $(\mathbf{1b})_2 \cdot Ba^{2+}$ arises from the intermolecular NOE.

3. Conclusions

Thus, the 15-crown-5-containing 1-hydroxyanthraquinone-imine dyes **1**, all except **1c**, undergo prototropic tautomerization in MeCN to exist as an equilibrated mixture of the imine and enamine isomers. The binding of an alkaline metal cation to the crown ether moiety of the tautomeric dye causes a shift of the equilibrium toward the imine isomer due to electron-withdrawal effect of the crowned metal cation on the amine nitrogen atom. This results in significant changes in the absorption spectrum of the dye. The sandwich-type 2:1 complexes formed by dyes **1** with strontium and barium cations show higher stability constants than the corresponding 1:1 complexes, with the $K_{2:1}/K_{1:1}$ ratio reaching a value of 10. This phenomenon is related to interchromophoric stacking interactions in the sandwich structures; the greater the number of short stacking contacts in the 2:1 complex, the higher the $K_{2:1}/K_{1:1}$ ratio.

4. Experimental

4.1 General methods

^1H and ^{13}C NMR spectra were measured on a Bruker AVANCE III 500 spectrometer. The solvent ($\text{MeCN-}d_3$ or CDCl_3) was used as the internal reference.³¹ Absorption spectra were recorded on a Specord M40 spectrophotometer. Chromatography was conducted on glass columns packed with silica gel (63–100 μm). Thin layer chromatography (TLC) was carried out on Silufol UV-254 plates. Elemental analysis was performed on a Vario MICRO Cube analyzer. IR spectra were recorded on a Bruker Vector 22 spectrophotometer in KBr pellets.

4.2 Materials

Acetonitrile (special purity grade, water content < 0.03%, v/v) was used without additional purification. Benzene and ethanol were dried over anhydrous CaCl_2 and CuSO_4 , respectively, followed by distillation *in vacuo*. $\text{Mg}(\text{ClO}_4)_2$, $\text{Ca}(\text{ClO}_4)_2$, $\text{Sr}(\text{ClO}_4)_2$, and $\text{Ba}(\text{ClO}_4)_2$ were dried *in vacuo* at 230 °C, and LiClO_4 , NaClO_4 , and KClO_4 were dried *in vacuo* at 170 °C.

4.3 Spectrophotometric titration (SPT)

Experiments were conducted in MeCN in 1 and 4.75 cm quartz cells with ground-in stoppers. In each SPT experiment, the total ligand concentration (C_L) was maintained constant, and the total metal concentration (C_M) varied incrementally from 0 up to 2 mM (for the system **1b**– $\text{Mg}(\text{ClO}_4)_2$, the C_M value varied up to 0.5 M). The C_M -dependent absorption spectra obtained for each of the ligand–metal perchlorate systems were subjected to global analysis using the methods described previously.²³ The complexation stoichiometry, the complex stability constants, and the absorption spectra of pure complexes were determined by globally fitting the SPT data to the appropriate complexation model (see the Results and Discussion section). For those systems, where 2:1 ligand–metal complexes were detected, the desired characteristics were obtained by globally fitting the SPT data from the two experiments conducted at different C_L values in 1 and 4.75 cm cells. When needed, a possible systematic error in the C_M/C_L ratio was taken into account by introducing one more variable parameter into the fitting procedure (in addition to the complex stability constants).²³ The standard deviations in the stability constants as the fitting parameters did not exceed 1%.

4.4 ^1H NMR titration

Experiments were conducted in $\text{MeCN-}d_3$ in 5 mm NMR tubes (Norell, 500 MHz). The systems studied were **B15C5**– $\text{Ba}(\text{ClO}_4)_2$ and **1b**– $\text{Ba}(\text{ClO}_4)_2$. In the case of **1b**, the initial solution contained both the ligand and $\text{Ba}(\text{ClO}_4)_2$ (5 mL, $C_L = 2$ mM, $C_M = 1$ mM). During the NMR titration, the value of C_L was maintained at the same level, and the value of C_M increased incrementally up to 32

mM. Because of a low solubility of free dye **1b** in MeCN-*d*₃, its NMR spectrum was measured separately at a smaller value of C_L . The NMR titration of B15C5 with Ba(ClO₄)₂ was carried out similarly, except that the C_M value increased from zero. The proton signals that demonstrated the most significant shifts and that could be assigned unambiguously were used in the subsequent calculations. The chemical shifts δ were estimated by fitting the proton signals to a sum of Lorentzian functions (after the baseline correction). The dependencies of δ on C_M obtained for different protons of the ligand were fitted globally to the 2:1 complexation model represented by Equations (1) and (3), using the assumption that

$$\delta = ([L] \delta_L + [L \cdot M^{n+}] \delta_{1:1} + 2[L_2 \cdot M^{n+}] \delta_{2:1}) / C_L \quad (5)$$

where δ_L , $\delta_{1:1}$, and $\delta_{2:1}$ are the proton chemical shifts of L, $L \cdot M^{n+}$, and $L_2 \cdot M^{n+}$, respectively. In these calculations, the stability constant $K_{2:1}$ was used as a variable parameter, whereas the constant $K_{1:1}$ was fixed at the value derived from the SPT measurements (Tables 1 and 2). A variation of the $K_{1:1}$ value by $\pm 30\%$ had insignificant effect on the calculated value of $K_{2:1}/K_{1:1}$.

4.5 Mass spectrometry

Mass spectra were acquired using a custom-built Ortho-TOF mass spectrometer,³² equipped with a custom-built electrosonic spray ionization (ESSI) source. Owing to the use of supersonic nebulizing gas (N₂), the ESSI technique provides very efficient desolvation of ionic species and narrow charge-state distributions.³³ The spectrometer provides ~ 10000 FWHM resolution. It contains two transport radio frequency quadrupoles (RFQ),³⁴ facilitating efficient declusterization and transfer of ions to the Ortho-TOF mass analyzer. The ions are transferred from atmospheric pressure region via a metal capillary (0.4 mm ID, 11 cm long) to the interface consisted of two RFQ ion guides. The electrical potential applied to the sample solution via a stainless steel union (connector) can be tuned between 0 and 3 kV. The sample solution was injected by a syringe pump with a flow rate of 1 $\mu\text{L min}^{-1}$.

4.6 Quantum-chemical calculations

The molecular structures of complexes $(\mathbf{1})_2 \cdot \text{Sr}^{2+}$ in MeCN were calculated as follows. First, various conformations of model complexes $(\mathbf{1})_2 \cdot \text{Na}^+$ in the gas phase were analyzed using the parameterized electronic structure model developed by Laikov³⁵ and implemented in the Priroda 14 program.³⁶ The sodium atom was used in these preliminary calculations because the method has no parameterization for strontium. For each complex, several most probable conformations were selected in which sodium atoms were replaced by strontium atoms to perform the subsequent DFT calculations using the ORCA 3.0 program package.³⁷ Geometry optimizations of complexes $(\mathbf{1})_2 \cdot \text{Sr}^{2+}$ were carried out using the BLYP functional^{38,39} with the def2-TZVP basis set,⁴⁰ the D3

dispersion correction,⁴¹ and the gCP counterpoise correction.⁴² The COSMO method⁴³ was used to simulate effects of MeCN as the experimental solvent.

4.7 Synthesis of precursors

Compound **2a** was prepared from 1-chloro-9,10-anthraquinone (**5**) according to the procedure described previously.⁴⁴ 4-(*tert*-Butyl)phenol (16 mmol) and KOH (8 mmol) were mixed with 4 mmol of **5** and a catalytic amount of metallic copper. The mixture was heated at 130 °C with stirring under reflux for 2 hours, then cooled to 100 °C and added to 50 mL of 10% aqueous KOH. The resulting yellow precipitate was filtered off and washed, first with 100 mL of 5% aqueous KOH and then with distilled water to neutral pH. The residue was dried and subjected to column chromatography on silica gel using toluene as the eluent. The second yellow fraction was collected, evaporated to dryness and then recrystallized from ethanol to give a flaky yellow solid (1.18 g, 81% yield). A similar procedure was used to prepare 2-, 4-, and 5-amino derivatives of **2a** (**6a–c**) from the corresponding amino derivatives of **5**. Benzoylation of **6a–c** resulted in compounds **2b–d**, respectively.⁴⁴ Compound **2e** was obtained by acylation of **6a** with trifluoroacetyl chloride. The ¹H NMR spectra of compounds **2** are presented in Figures S18–S23. 4'-Aminobenzo-15-crown-5 ether (**3**) was prepared by Pd/C-catalyzed reduction of 4'-nitrobenzo-15-crown-5 ether by hydrazine hydrate in diethylene glycol dimethyl ether.⁴⁵

4.8 Synthesis of dyes **1a–e** (general method)

1-Aryloxy-9,10-anthraquinone **2** (0.20 mmol) was dissolved in dry benzene (100 mL), then crown ether **3** (0.25 mmol) was added, and the solution was exposed to sunlight for 6–8 hours until compound **2** was completely consumed (monitoring by TLC). The reaction mixture was evaporated *in vacuo* at 40 °C. The residue was washed with hexane, filtered off, and dissolved in benzene (15 mL). The solution was subjected to column chromatography on silica gel. First, yellow by-product (1-hydroxyanthraquinone) was separated by elution with benzene. Then a deep colored fraction containing compound **1** was collected by elution with a 3:1 benzene–ethanol mixture; the solvent was evaporated *in vacuo* at 40 °C and the residue was recrystallized from a 1:1 benzene–ethanol mixture.

4-Hydroxy-10-((2,3,5,6,8,9,11,12-octahydrobenzo[*b*][1,4,7,10,13]pentaoxacyclopentadecin-15-yl)imino)anthracen-9(10*H*)-one (1a**).** Compound **1a** was obtained as an orange solid (0.069 g, 71%); m.p. 125–127 °C. ¹H NMR (500 MHz, CDCl₃, Fig. S24): δ = 14.88 (s, 1H; OH), 8.30 (dd, *J* = 7.8, 1.5 Hz, 1H; 5-H), 7.82 (dd, *J* = 7.6, 1.3 Hz, 1H; 8-H), 7.51–7.58 (m, 2H; 6,7-H), 7.48 (dd, *J* = 8.2, 1.2 Hz, 1H; 4-H), 7.33–7.36 (m, 1H; 3-H), 7.31 (dd, *J* = 8.2, 1.2 Hz, 1H; 2-H), 6.88 (d, *J* = 8.4 Hz, 1H; 5'-H), 6.57 (d, *J* = 2.4

Hz, 1H; 2'-H), 6.53 (dd, $J = 8.4, 2.4$ Hz, 1H; 6'-H), 4.15–4.20 (m, 2H; α -H), 4.02–4.08 (m, 2H; α' -H), 3.93–3.97 (m, 2H; β -H), 3.86–3.91 (m, 2H; β' -H), 3.71–3.83 (m, 8H; $\gamma, \delta, \delta', \gamma'$ -H) ppm. ^{13}C NMR (500 MHz, CDCl_3 , Fig. S25): $\delta = 183.74$ (10-C), 161.45 (9-C), 159.53 (1-C), 150.48 (3'-C), 147.18 (4'-C), 141.76 (1'-C), 134.03 (12-C), 132.94 (11-C), 132.37 (7-C), 132.31 (6-C), 132.01 (14-C), 130.01 (13-C), 129.48 (8-C), 128.08 (5-C), 124.11 (3-C), 118.47 (2-C), 118.22 (4-C), 115.03 (5'-C), 112.57 (6'-C), 106.47 (2'-C), 71.17 (δ -C), 71.10 (δ' -C), 70.51 (γ -C), 70.41 (γ' -C), 69.66 (β -C), 69.40 (β' -C), 69.32 (α -C), 68.85 (α' -C) ppm. IR (KBr) $\tilde{\nu}$ [cm^{-1}]: 3439 (OH), 3073 (CH_{ar}), 2924, 2856 (CH_2), 1665 (C=O), 1591 (C=N), 1555, 1512 (C=C_{ar}). ESI-MS: m/z calcd for $\text{C}_{28}\text{H}_{27}\text{NO}_7 + \text{H}^+$: 490.186 [$M + \text{H}^+$]; found: 490.194. Elemental analysis calcd (%) for $\text{C}_{28}\text{H}_{27}\text{NO}_7$: C 68.70, H 5.56, N 2.86; found: C 68.61, H 5.62, N 2.90.

***N*-(1-Hydroxy-9-((2,3,5,6,8,9,11,12-octahydrobenzo[*b*][1,4,7,10,13]pentaoxacyclopentadecin-15-yl)imino)-10-oxo-9,10-dihydroanthracen-2-yl)benzamide (1b).** Compound **1b** was obtained as a brown powder (0.089 g, 73%); m.p. 157–159 °C. ^1H NMR (500 MHz, $\text{MeCN-}d_3$ - CDCl_3 (4:1), Fig. S26): $\delta = 16.57$ (s, 1H; OH), 9.18 (s, 1H; NH), 8.74 (d, $J = 8.4$ Hz, 1H; 4-H), 8.28 (dd, $J = 7.8, 1.2$ Hz, 1H; 5-H), 7.94–7.98 (m, 2H; 2'',6''-H), 7.82 (d, $J = 8.4$ Hz, 1H; 3-H), 7.60–7.69 (m, 2H; 6,7-H), 7.54–7.58 (m, 2H; 3'',5''-H), 7.51 (d, $J = 8.2, 1.1$ Hz, 1H; 8-H), 7.39 (td, $J = 7.3, 1.5$ Hz, 1H; 4''-H), 7.11 (d, $J = 8.4$ Hz, 1H; 5'-H), 6.91 (d, $J = 2.3$ Hz, 1H; 2'-H), 6.82 (dd, $J = 8.4, 2.3$ Hz, 1H; 6'-H), 4.22–4.29 (m, 2H; α -H), 4.07–4.15 (m, 2H; α' -H), 3.89–3.96 (m, 2H; β -H), 3.81–3.87 (m, 2H; β' -H), 3.68–3.81 (m, 8H; $\gamma, \gamma', \delta, \delta'$ -H) ppm. ^{13}C NMR (500 MHz, $\text{MeCN-}d_3$ - CDCl_3 (4:1), Fig. S28): $\delta = 182.86$ (10-C), 166.33 (NHCO), 161.82 (9-C), 154.42 (1-C), 149.36 (3'-C), 146.56 (4'-C), 141.57 (1'-C), 135.47 (2-C), 135.42 (12-C), 135.17 (1''-C), 133.80 (7-C), 133.34 (6-C), 133.08 (4''-C), 130.44 (8-C), 129.98 (3'',5''-C), 129.25 (11-C), 128.75 (5-C), 128.20 (2'',6''-C), 127.31 (14-C), 126.29 (13-C), 122.26 (4-C), 119.56 (3-C), 116.25 (5'-C), 115.63 (6'-C), 108.57 (2'-C), 69.67 (δ -C), 69.65 (δ' -C), 69.12 (γ -C), 69.04 (γ' -C), 68.75 (β, β' -C), 68.57 (α, α' -C) ppm. IR (KBr) $\tilde{\nu}$ [cm^{-1}]: 3431, 3378 (OH, NH), 3073 (CH_{ar}), 2912, 2866 (CH_2), 1671 (C=O), 1653 (C=N), 1590, 1513 (C=C_{ar}). ESI-MS: m/z calcd for $\text{C}_{35}\text{H}_{32}\text{N}_2\text{O}_8 + \text{H}^+$: 609.223 [$M + \text{H}^+$]; found: 609.260. Elemental analysis calcd (%) for $\text{C}_{35}\text{H}_{32}\text{N}_2\text{O}_8$: C 69.07, H 5.30, N 4.60; found: C 69.07, H 5.66, N 4.49.

***N*-(4-Hydroxy-10-((2,3,5,6,8,9,11,12-octahydrobenzo[*b*][1,4,7,10,13]pentaoxacyclopentadecin-15-yl)imino)-9-oxo-9,10-dihydroanthracen-1-yl)benzamide (1c).** Compound **1c** was obtained as a dark red powder (0.071 g, 58%); m.p. 161–163 °C. ^1H NMR (500 MHz, CDCl_3 , Fig. S29): $\delta = 15.58$ (s, 1H; OH), 13.28 (s, 1H; NH), 9.16 (d, $J = 9.4$ Hz, 1H; 3-H), 8.36 (dd, $J = 7.9, 1.4$ Hz, 1H; 5-H), 8.14–8.18 (m, 2H; 2'',6''-H), 7.55–7.62 (m, 4H; 6,7,3'',5''-H), 7.50 (d, $J = 8.1$ Hz, 1H; 8-H), 7.44 (d, $J = 9.4$ Hz, 1H; 2-

H), 7.33–7.40 (m, 1H; 4''-H), 6.88 (d, $J = 8.4$ Hz, 1H; 5'-H), 6.61 (d, $J = 2.4$ Hz, 1H; 2'-H), 6.55 (dd, $J = 8.4, 2.4$ Hz, 1H; 6'-H), 4.15–4.20 (m, 2H; $2 \times \alpha$ -H), 4.03–4.09 (m, 2H; $2 \times \alpha'$ -H), 3.93–3.98 (m, 2H; $2 \times \beta$ -H), 3.87–3.92 (m, 2H; $2 \times \beta'$ -H), 3.74–3.84 (m, 8H; $2 \times \gamma$ -H, $2 \times \gamma'$ -H, $2 \times \delta$ -H, $2 \times \delta'$ -H) ppm. ^{13}C NMR (500 MHz, CDCl_3 , Fig. S30): $\delta = 187.27$ (10-C), 166.38 (NHCO), 159.36 (9-C), 158.58 (1-C), 150.51 (3'-C), 147.36 (4'-C), 141.25 (1'-C), 135.81 (4-C), 135.13 (12-C), 134.51 (11-C), 132.51 (14-C), 132.16 (1''-C), 132.10 (13-C), 129.30 (4''-C), 129.21 (7-C), 129.00 (3'',5''-C), 128.30 (6-C), 127.75 (2'',6''-C), 127.69 (8-C), 126.78 (5-C), 116.49 (3-C), 116.36 (2-C), 114.96 (5'-C), 113.00 (6'-C), 106.83 (2'-C), 71.16 (δ -C), 71.11 (δ' -C), 70.49 (γ -C), 70.40 (γ' -C), 69.63 (β -C), 69.39 (β' -C), 69.28 (α -C), 68.88 (α' -C) ppm. IR (KBr) $\tilde{\nu}$ [cm^{-1}]: 3356, 3308 (OH, NH), 3062 (CH_{ar}), 2950, 2921 (CH_2), 1671, 1630 (C=O, C=N), 1601, 1582 (C=C_{ar}). ESI-MS: m/z calcd for $\text{C}_{35}\text{H}_{32}\text{N}_2\text{O}_8 + \text{H}^+$: 609.223 [$M + \text{H}^+$]; found: 609.242. Elemental analysis calcd (%) for $\text{C}_{35}\text{H}_{32}\text{N}_2\text{O}_8$: C 69.07, H 5.30, N 4.60; found: C 68.77, H 5.31, N 4.65.

***N*-(5-Hydroxy-10-((2,3,5,6,8,9,11,12-octahydrobenzo[*b*][1,4,7,10,13]pentaoxacyclopentadecin-15-yl)imino)-9-oxo-9,10-dihydroanthracen-1-yl)benzamide (1d).** Compound **1d** was obtained as a dark red powder (0.078 g, 64%); m.p. 163–165 °C. ^1H NMR (500 MHz, CDCl_3 , Fig. S31): $\delta = 14.57$ (s, 1H; OH), 13.34 (s, 1H; NH), 9.11 (dd, $J = 8.4, 1.1$ Hz, 1H; 8-H), 8.14–8.19 (m, 2H; 2'',6''-H), 7.82 (dd, $J = 7.6, 1.1$ Hz, 1H; 6-H), 7.56–7.65 (m, 3H; 3'',4'',5''), 7.54 (t, $J = 8.0$ Hz, 1H; 7-H), 7.39 (t, $J = 8.2$ Hz, 1H; 3-H), 7.29–7.34 (m, 2H; 2,4-H), 6.86 (d, $J = 8.4$ Hz, 1H; 5'-H), 6.56 (d, $J = 2.3$ Hz, 1H; 2'-H), 6.54 (dd, $J = 8.4, 2.3$ Hz, 1H; 6'-H), 4.15–4.20 (m, 2H; $2 \times \alpha$ -H), 4.03–4.09 (m, 2H; $2 \times \alpha'$ -H), 3.93–3.98 (m, 2H; $2 \times \beta$ -H), 3.87–3.92 (m, 2H; $2 \times \beta'$ -H), 3.74–3.84 (m, 8H; $2 \times \gamma$ -H, $2 \times \gamma'$ -H, $2 \times \delta$ -H, $2 \times \delta'$ -H) ppm. ^{13}C NMR (500 MHz, CDCl_3 , Fig. S32): $\delta = 188.15$ (10-C), 166.60 (NHCO), 160.74 (9-C), 159.35 (1-C), 150.46 (3'-C), 142.45 (4'-C), 141.61 (1'-C), 134.76 (5-C), 133.94 (12-C), 133.09 (14-C), 132.95 (11-C), 132.43 (13-C), 131.05 (1''-C), 129.17 (4''-C), 129.09 (3'',5''-C), 127.80 (2'',6''-C), 124.86 (3-C), 124.01 (7-C), 123.82 (8-C), 118.79 (4-C), 118.71 (6-C), 117.76 (2-C), 116.49 (5'-C), 113.15 (6'-C), 106.84 (2'-C); 71.18 (δ -C), 71.12 (δ' -C), 70.53 (γ -C), 70.45 (γ' -C), 69.64 (β -C), 69.40 (β' -C), 69.28 (α -C), 68.92 (α' -C) ppm. ESI-MS: m/z calcd for $\text{C}_{35}\text{H}_{32}\text{N}_2\text{O}_8 + \text{H}^+$: 609.223 [$M + \text{H}^+$]; found: 609.248. Elemental analysis calcd (%) for $\text{C}_{35}\text{H}_{32}\text{N}_2\text{O}_8$: C 69.07, H 5.30, N 4.60; found: C 68.82, H 5.32, N 4.68.

2,2,2-Trifluoro-*N*-(1-hydroxy-9-((2,3,5,6,8,9,11,12-octahydrobenzo[*b*][1,4,7,10,13]pentaoxacyclopentadecin-15-yl)imino)-10-oxo-9,10-dihydroanthracen-2-yl)acetamide (1e). Compound **1e** was obtained as a dark red powder (0.089 g, 74%); m.p. 153–155 °C. ^1H NMR (500 MHz, CDCl_3 , Fig. S33): $\delta = 17.34$ (s, 1H; OH), 9.35 (s, 1H; NH), 8.58 (d, $J = 8.3$ Hz, 1H; 3-H), 8.35 (dd, $J = 7.8, 1.1$ Hz, 1H; 5-H), 7.82 (d, $J = 8.3$ Hz, 1H;

4-H), 7.63 (td, $J = 7.8, 1.1$ Hz, 1H; 6-H), 7.56 (dd, $J = 8.2, 1.0$ Hz, 1H; 8-H), 7.38 (td, $J = 7.8, 1.5$ Hz, 1H; 7-H), 6.92 (d, $J = 8.5$ Hz, 1H; 5'-H), 6.66–6.71 (m, 2H; 2',6'-H), 4.17–4.22 (m, 2H; α -H), 4.03–4.09 (m, 2H; α' -H), 3.94–3.99 (m, 2H; β -H), 3.87–3.92 (m, 2H; β' -H), 3.74–3.83 (m, 8H; $\gamma, \gamma', \delta, \delta'$ -H) ppm. ^{13}C NMR (500 MHz, CDCl_3 , Fig. S35): $\delta = 181.94$ (10-C), 160.16 (9-C), 156.25 (NHCO), 154.84 (1-C), 150.58 (3'-C), 148.38 (4'-C), 137.65 (1'-C), 134.50 (2-C), 133.11 (7-C), 132.50 (6-C), 131.96 (11-C), 129.38 (8-C), 129.12 (12-C), 128.62 (5-C), 128.36 (14-C), 127.77 (13-C), 122.18 (4-C), 118.49 (3-C), 115.14 (CF_3), 114.66 (5'-C), 114.21 (6'-C), 107.53 (2'-C), 71.17 (δ -C), 71.13 (δ' -C), 70.42 (γ -C), 70.37 (γ' -C), 69.52 (β -C), 69.32 (β' -C), 69.15 (α -C), 68.98 (α' -C) ppm. IR (KBr) $\tilde{\nu}$ [cm^{-1}]: 3333 (OH, NH), 3075 (C-H_{ar}), 2932, 2860 (C-H), 1719 (C=O in NHCOCF_3), 1655 (C=O , C=N), 1588 (C=C_{ar}), 1541, 1510 (C=C_{ar}), 1129 (CF_3). ESI-MS: m/z calcd for $\text{C}_{30}\text{H}_{27}\text{F}_3\text{N}_2\text{O}_8+\text{H}^+$: 601.179 [$M+\text{H}^+$]; found: 601.170. Elemental analysis calcd (%) for $\text{C}_{30}\text{H}_{27}\text{F}_3\text{N}_2\text{O}_8$: C 60.00, H 4.53, N 4.66; found: C 59.86, H 4.42, N 4.81.

Acknowledgments

The authors thank Dr. A. V. Chernyak for his assistance with NMR experiments.

Supplementary data

Supplementary data related to this article can be found at <http://dx.doi.org/...>

References

1. Antonov L. *Tautomerism: Methods and Theories*; Wiley-VCH: Weinheim, 2014. doi:10.1002/9783527658824
2. Izatt, R. M.; Pawlak, K.; Bradshaw, J. S.; Bruening, R. L. *Chem. Rev.* **1991**, *91*, 1721–2085. doi:10.1021/cr00008a003
3. Shinkai, S. *Pure Appl. Chem.* **1987**, *59*, 425–430. doi:10.1351/pac198759030425
4. Ushakov, E. N.; Alfimov, M. V.; Gromov, S. P. *Macroheterocycles* **2010**, *3*, 189–200. doi:10.6060/mhc2010.4.189
5. Natali, M.; Giordani, S. *Chem. Soc. Rev.* **2012**, *41*, 4010–4029. doi:10.1039/c2cs35015g
6. Löhr, H.-G.; Vögtle, F. *Acc. Chem. Res.* **1985**, *18*, 65–72. doi:10.1021/ar00111a001
7. de Silva, A. P.; Gunaratne, H. Q. N.; Gunnlaugsson, T.; Huxley, A. J. M.; McCoy, C. P.; Rademacher, J. T.; Rice, T. E. *Chem. Rev.* **1997**, *97*, 1515–1566. doi:10.1021/cr960386p
8. Chapoteau, E.; Czech, B. P.; Gebauer, C. R.; Kumar, A.; Leong, K.; Mytych, D. T.; Zazulak, W.; Desai, D. H.; Luboch, E.; Krzykawski, J.; Bartsch, R. A. *J. Org. Chem.* **1991**, *56*, 2575–2579. doi:10.1021/jo00007a057
9. Hayvali, Z.; Hayvali, M.; Kiliç, Z.; Hökelek, T.; Weber, E. *J. Incl. Phen. Macrocycl. Chem.* **2003**, *45*, 285–294. doi:10.1023/A:1024568309739
10. Dubonosov, A. D.; Minkin, V. I.; Bren, V. A.; Shepelenko, E. N.; Tsukanov, A. V.; Starikov, A. G.; Borodkin, G. S. *Tetrahedron* **2008**, *64*, 3160–3167. doi:10.1016/j.tet.2008.01.096
11. Deneva, V.; Burdzhiev, N.; Stanoeva, E.; Antonov, L. *Spectrosc. Lett.* **2010**, *43*, 22–27. doi:10.1080/00387010903260273
12. Antonov, L. M.; Kurteva, V. B.; Simeonov, S. P.; Deneva, V. V.; Crochet, A.; Fromm, K. M. *Tetrahedron* **2010**, *66*, 4292–4297. doi:10.1016/j.tet.2010.04.049
13. Gritsan, N. P.; Klimenko, L. S.; Leonenko, Z. V.; Mainagashev, I. Ya.; Mamatyuk, V. I.; Vetchinov, V. P. *Tetrahedron* **1995**, *51*, 3061–3076. doi:10.1016/0040-4020(95)00046-B
14. Yatsenko, A. V.; Tafeenko, V. A.; Zhukov, S. G.; Medvedev, S. V.; Popov, S. I. *Struct. Chem.* **1997**, *8*, 197–204. doi:10.1007/BF02263507
15. Martyanov, T. P.; Ushakov, E. N.; Savelyev, V. A.; Klimenko, L. S. *Russ. Chem. Bull.* **2012**, *61*, 2282–2294. doi:10.1007/s11172-012-0323-z
16. Pedersen, C. J. *J. Am. Chem. Soc.* **1970**, *92*, 386–391. doi:10.1021/ja00705a605
17. An, H.; Bradshaw, J. S.; Izatt, R. M.; Yan, Z. *Chem. Rev.* **1994**, *94*, 939–991. doi:10.1021/cr00028a005
18. Fery-Forgues, S.; Al-Ali, F. *J. Photochem. Photobiol. C: Photochem. Rev.* **2004**, *5*, 139–153. doi:10.1016/j.jphotochemrev.2004.07.001

19. Sherman, C. L.; Brodbelt, J. S.; Marchand, A. P.; Poola, B. *J. Am. Soc. Mass Spectrom.* **2005**, *16*, 1162–1171. doi:10.1016/j.jasms.2005.03.014
20. Frański, R.; Gierczyk, B. *J. Am. Soc. Mass Spectrom.* **2010**, *21*, 545–549. doi:10.1016/j.jasms.2009.12.018
21. Klimenko, L. S.; Kusov, S. Z.; Vlasov, V. M. *Mendeleev Commun.* **2002**, *12*, 102–103. doi:10.1070/MC2002v012n03ABEH001592
22. Klimenko, L. S.; Kusov, S. Z.; Vlasov, V. M.; Tchabueva, E. N.; Boldyrev, V. V. *Mendeleev Commun.* **2006**, *16*, 224–225. doi:10.1070/MC2006v016n04ABEH002294
23. Ushakov, E. N.; Gromov, S. P.; Fedorova, O. A.; Pershina, Yu. V.; Alfimov, M. V.; Barigilletti, F.; Flamigni, L.; Balzani, V. *J. Phys. Chem. A* **1999**, *103*, 11188–11193. doi:10.1021/jp9929420
24. Arnaud-Neu, F.; Delgado, R.; Chaves, S. *Pure Appl. Chem.* **2003**, *75*, 71–102. doi:10.1351/pac200375010071
25. Shannon, R. D. *Acta Cryst.* **1976**, *A32*, 751–767. doi:10.1107/S0567739476001551
26. Gromov, S. P.; Vedernikov, A. I.; Ushakov, E. N.; Kuz'mina, L. G.; Feofanov, A. V.; Avakyan, V. G.; Churakov, A. V.; Alaverdyan, Yu. S.; Malysheva, E. V.; Alfimov, M. V.; Howard, J. A. K.; Eliasson, B.; Edlund, U. G. *Helv. Chim. Acta* **2002**, *85*, 60–81. doi:10.1002/1522-2675(200201)85:1<60::AID-HLCA60>3.0.CO;2-C
27. Schmidt, A.; Karas, M.; Dülcks, T. *J. Am. Soc. Mass Spectr.* **2003**, *14*, 492–500. doi:10.1016/S1044-0305(03)00128-4
28. Kempen, E. C.; Brodbelt, J. S. *Anal. Chem.* **2000**, *72*, 5411–5416. doi:10.1021/ac000540e
29. Nakamura, M.; Fujioka, T.; Sakamoto, H.; Kimura, K. *New J. Chem.* **2002**, *26*, 554–559. doi:10.1039/B111016K
30. Nakamura, M.; Takahashi, K.; Fujioka, T.; Kado, S.; Sakamoto, H.; Kimura, K. *J. Am. Soc. Mass Spectr.* **2003**, *14*, 1110–1115. doi:10.1016/S1044-0305(03)00447-1
31. Gottlieb, H. E.; Kotlyar, V.; Nudelman, A. *J. Org. Chem.* **1997**, *62*, 7512–7515. doi:10.1021/jo971176v
32. Dodonov, A. F.; Loboda, A. V.; Kozlovski, V. I.; Soulimenkov, I. V.; Raznikov, V. V.; Zhen, Z.; Horwath, T.; Wollnik, H. *Eur. J. Mass Spectrom.* **2000**, *6*, 481–490. doi:10.1255/ejms.378
33. Hirabayashi, A.; Sakairi, M.; Takada, Ya.; Koizumi, H. *Trends Anal. Chem.* **1997**, *16*, 45–52. doi:10.1016/S0165-9936(96)00078-7
34. Dodonov, A.; Kozlovski, V.; Loboda, A.; Raznikov, V.; Sulimenkov, I.; Tolmachev, A.; Kraft, A.; Wollnik, H. *Rapid Commun. Mass Spectrom.* **1997**, *11*, 1649–1656. doi:10.1002/(SICI)1097-0231(19971015)11:15<1649::AID-RCM67>3.0.CO;2-T
35. Laikov, D. N. *J. Chem. Phys.* **2011**, *135*, 134120–134130. doi:10.1063/1.3646498

36. Laikov, D. N. *Priroda, Quantum Chemical Program*, Version 2014.02.23; Lomonosov Moscow State University, Moscow, 2014.
37. Neese, F. *WIREs Comput. Mol. Sci.* **2012**, *2*, 73–78. doi:10.1002/wcms.81
38. Becke, A. D. *Phys. Rev. A* **1988**, *38*, 3098–3100. doi:10.1103/PhysRevA.38.3098
39. Lee, C.; Yang, W.; Parr, R. G. *Phys. Rev. B* **1988**, *37*, 785–789. doi:10.1103/PhysRevB.37.785
40. Weigend, F.; Ahlrichs, R. *Phys. Chem. Chem. Phys.* **2005**, *7*, 3297–3305. doi:10.1039/B508541A
41. Grimme, S.; Antony, J.; Ehrlich, S.; Krieg, H. *J. Chem. Phys.* **2010**, *132*, 154104–154119. doi:10.1063/1.3382344
42. Kruse, H.; Grimme, S. *J. Chem. Phys.* **2012**, *136*, 154101–153116. doi:10.1063/1.3700154
43. Klamt, A.; Schüürmann, G. *J. Chem. Soc., Perkin Trans. 2* **1993**, 799–805. doi:10.1039/P29930000799
44. Fokin, E. P.; Russkikh, S. A.; Klimenko, L. S. *Izv. Sib. Otd. Akad. Nauk SSSR, Ser. Khim. Nauk.* **1979**, *9*, 117–124 (in Russian).
45. Berezina, R. N.; Kobrin, V. S.; Kusov, S. Z.; Lubenets, E. G. *Zh. Org. Khim.* **1998**, *34*, 1581–1582; *Russ. J. Org. Chem.* **1998**, *34*, 1517–1518.